



Mechanical impact on a breath figure

Lorenzo Betti , Céline Cohen, ^{*} and Xavier Noblin [†]*Université Côte d'Azur, CNRS UMR 7010, Institut de Physique de Nice (INPHYNI), Site Valrose, Av. Vallot, 06108 Nice Cedex 2, France*

(Received 29 March 2022; accepted 10 October 2022; published 9 January 2023; corrected 27 January 2023)

We present here the effect of mechanical vibrations on a breath figure. By impacting a falling steel ball on a plastic plate covered on its bottom side by a breath figure, we show that in a few milliseconds, the figure can evolve even more dramatically than it would in minutes in the natural aging process. We quantify the variations of droplet number and sizes with time for various substrate accelerations and mean initial droplets radii. We show that, above an acceleration threshold, the final number of droplets decreases more and more with acceleration. We interpret this result by the contact line unpinning provoking oscillations of the droplets radii, which makes the drops contact and coalesce with neighbors. Finally, we introduce a new parameter to characterize the droplet number decrease. We have plotted it as a function of an effective Bond number built with the substrate acceleration and mean droplet radius. Interestingly, all the data fall on a single master curve.

DOI: [10.1103/PhysRevFluids.8.013601](https://doi.org/10.1103/PhysRevFluids.8.013601)

I. INTRODUCTION

A breath figure describes the droplet pattern formed when water vapor condenses onto a cold surface in a humid environment. The evolution of breath figure in time has been actively studied experimentally and numerically during the last decades [1,2], motivated by understanding droplet growth [3,4], thin film vapor deposition [5], or improving other applied systems [6,7] such as dew recovery systems [8]. The recovery of dew water is indeed nowadays of a crucial environmental interest for water delivery in arid regions [9,10].

Dew formation can be also problematic for industrial application. It can affect visibility through a transparent surface and produce security or aesthetic issues: cars' windshields, supermarket freezer's doors, or eyeglasses. To minimize these problems several directions can be followed. One can dry the air [11], make a treatment that limits the nucleation of droplets, or collect the droplets by moving them away from the surface using gravity, helped eventually by an adapted surface treatment to make their motion easier [12–16].

The breath figure's growth kinetics can be followed by measuring the droplets radii over time [2]. First, nanometric droplets of spherical cap shape are formed by heterogeneous nucleation. During the moment just after droplets nucleation, drops grow individually without coalescence and their mean radii increase initially with time following a power law: $\langle R \rangle \propto t^{\frac{1}{2}}$ as they are independent, then $\langle R \rangle \propto t^{\frac{1}{3}}$ when the vapor concentration profile around them overlap. After a certain time, when drops are larger and close enough, they start to coalesce with each other and the mean radius evolution with time becomes linear: $\langle R \rangle \propto t$ [1,2,10].

^{*}celine.cohen@unice.fr

[†]xavier.noblin@unice.fr

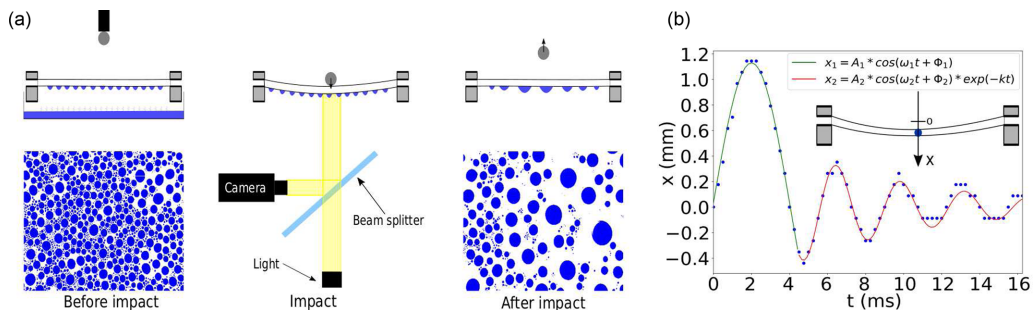


FIG. 1. (a) left: side and top view before impact; center: Experimental setup to impact a solid projectile on the back of a solid substrate that is covered with a breath figure and side view at the moment of impact; right: side and top view after impact. (b) Measured motion of the substrate’s center induced by the impact of the projectile.

The influence of the substrate’s wettability, roughness, and geometry on breath figure evolution have been explored in different studies [17–19]. They show that the droplet growth can be enhanced or reduced, by geometric or thermal discontinuities [20]. In addition, when drops are large enough, they will slide on a vertical or inclined surface due to gravity [21,22] which is particularly useful for collecting water [8].

In order to rapidly increase drop size without waiting for the natural growth, it can be interesting to solicit directly the droplets to trigger the coalescence. Inducing the coalescence of two droplets has already been studied in literature from the fundamental point of view [23,24] and used to trigger the mixing of two liquids to study a chemical reaction [25], for example. Furthermore, it has been also demonstrated that vibrations or electrowetting allow moving the contact line of a sessile droplet [26,27] on a substrate in a controlled way, but also the whole droplet [28–30].

The aim of the present study is to explore how mechanical vibrations of a solid substrate impacts the coalescence of droplets and modify the breath figure evolution. The aim is to accelerate the natural evolution of the breath figure towards larger drops which will more easily slide away from the surface.

Here, we developed a simple way to induce vibration of a solid surface with high acceleration by impacting a solid projectile on a substrate that is covered on the back by a breath figure. We have studied in detail the evolution of the drop mean radius and the drop number over time during an impact for different heights of a falling projectile and a different location on the surface from the impacting point.

We present first in this manuscript the experimental setup, its characterization, and the image analysis method. The vibration of the plate was determined as the function of the impact height and the observed zone on the plate. This gives us a tool to vary the acceleration felt by the droplets. Then, we present the influence of the acceleration on the size distribution and the droplet number of a breath figure after an impact.

II. MATERIALS AND METHODS

The experimental setup is schematized in Fig. 1(a). A breath figure is obtained by exposing a substrate facing down toward the vapor of a hot deionized water reservoir during a given time. Then the reservoir is removed just before the onset of impact. A solid magnetic ball ($m = 60$ g, $\varnothing = 2.5$ cm), named projectile, is dropped above the center of the substrate, by turning off an electromagnet disposed just above it at a chosen height H . The substrate is clamped by two metallic pieces screwed regularly, all along its edges, to ensure axisymmetrical deformations. A fast camera aligned with a beamsplitter under the substrate, allows the capture of images of the condensed drops during the experiment from below. The substrate is illuminated with a fiber optics illuminator (Edmundoptics) through the beamsplitter.

The substrate is an industrial polycarbonate (PC) circular plate of diameter $d = 14$ cm and thickness $h = 3$ mm. Its wetting properties are characterized by measuring the advancing θ_a and receding θ_r contact angles using a classical sessile drop technique using a homemade apparatus with a vertical syringe tip connected to a precise syringe pump to increase and decrease the volume of the droplet. The side view and image analysis of the droplets lead to the measurement of the wetting angles (advancing, receding) at very low speed (of order $1 \mu\text{m/s}$). The difference between these two angles is defined as the contact angle hysteresis of the surface ($\Delta\theta = \theta_a - \theta_r$) and it informs of the ability of the drop to move on the surface. Indeed, drops can be easily displaced on surfaces presenting low contact angle hysteresis. In our case, the results are $\theta_a = 85.3 \pm 0.5^\circ$, $\theta_r = 61.9 \pm 1.6^\circ$, and $\Delta\theta = 23.4 \pm 2^\circ$.

Motions of the substrate induced by the impact of the projectile have been characterized as a function of the position on the substrate from the impacting point by observing the motion of millimetric pillars stuck at different positions on the surface. For each position, we have plotted the vertical displacement of the pillar bottom x_i as the function of time. In addition, for each position on the surface, for a given dropping height, we observe a uniform vibration of the pillars at the same frequency; only the amplitude varies, hence the plate oscillates at its first mode. A typical result is presented in Fig. 1(b). The signal is composed of two parts. The first part is an arched curve larger and higher than the next ones, representing the impact, when the metallic ball is in contact with the substrate. The second part of the signal corresponds to the free vibration of the substrate, when the projectile has left the substrate. This part can be fitted respectively by $x_1 = A_1 * \cos(\omega_1 t + \Phi_1)$ (green) and by $x_2 = A_2 * \cos(\omega_2 t + \Phi_2) * \exp(-kt)$ (red) with A_1 and A_2 the respective amplitudes, ω_1 and ω_2 the respective pulsations, Φ_1 and Φ_2 the phases, and k . We determine the two pulsations $\omega_1 < \omega_2$ (corresponding frequencies of 125 Hz for the green part and 315 Hz for the red part). The difference between the two pulsations comes from the presence of an additional mass during impact (the metallic ball), corresponding to a higher effective mass of the plate. The eigenfrequencies of a clamped circular plate can be calculated for the first mode as [31] $\omega_p = 40.858 \sqrt{\frac{Eh^2}{\rho d^4 12(1-\nu^2)}}$, where E is the Young's modulus, ρ the density, h the thickness, d the diameter, and ν the Poisson ratio. When the ball is in contact with the plate, the frequency can be rewritten as $\omega_B = 40.858 \sqrt{\frac{\pi E h^3}{48(1-\nu^2)d^2(M_p + M_B)}}$. M_p is the mass of the plate and M_B is the mass of the ball. Then indeed, increasing the mass implies a decrease of ω ; it explains the two frequencies measured ω_1 and ω_2 . Since the main part of the vibration coalescence phenomenon occurs at impact, we have chosen to use only A_1 , ω_1 to characterize the impact. Derivating two times this signal allowed deduction of the acceleration of the substrate at the moment of impact t_{impact} by $\ddot{x}_1(t_{\text{impact}}) = A_1 \omega_1^2 = a_1$.

The film from the high-speed camera was obtained at 4000 fps. The image analysis was carried out on the software ImageJ using a threshold method to distinguish droplets. Figure 1(a) presents two treated images of a breath figure (before and after impact). We measure on those images the number of droplets, the wetted area, and the droplet size distribution. As it is classically observed for breath figure, the initial droplet size distribution is bimodal, with a distribution of small and large droplets [2]. The small droplets are linked to new nucleation events between larger drops that are sufficiently far apart to prevent the overlap of their water vapor concentration profiles. The large droplets are linked to the initial nucleation events and have grown more, eventually also by coalescence. We have chosen to identify the breath figures by the mean contact radius of this later category, the larger droplets R_m . We set a minimum droplet area for the detection by the software around 0.03 mm^2 . The mean covered area is obtained by the following formula: $\langle S \rangle = \frac{\sum s_i}{N}$, where s_i is the contact area of the droplet i and N is the total number of droplets. The mean contact radius is converted from $\langle S \rangle$ by $R_m = \sqrt{\frac{\langle S \rangle}{\pi}}$. This measurement R_m is used as a criteria for the breath figure aging. In the case discussed later where the droplets are not exactly circular after the impact effects, but elliptical, the mean radius R_m calculated is still a very good parameter of the new drop sizes, simply being the geometrical average of small and large axes of such elliptical droplets.

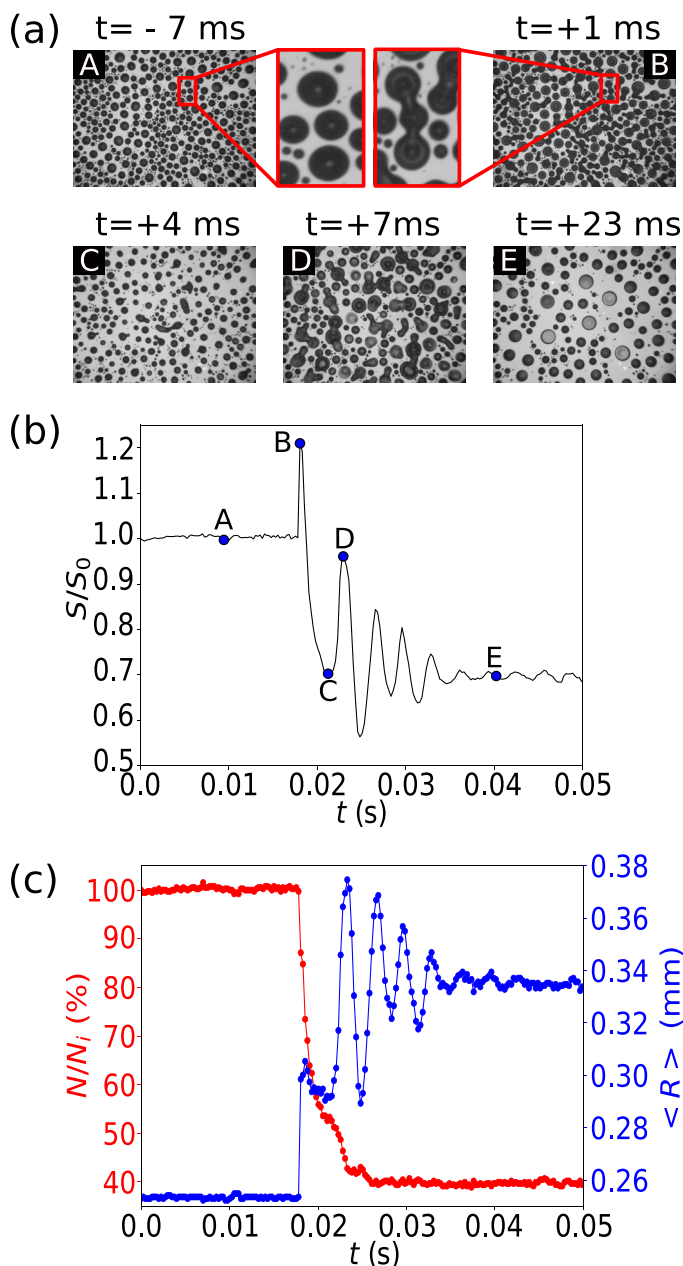


FIG. 2. (a) Breath figure key moments images during a typical experiment. The time corresponds to delay after impact. (b) Evolution of the total wetted area S normalized by the initial wetted area S_0 as a function of time corresponding to the images above. (c) Relative number of droplets in percent of the initial value (red) and average droplet contact radius as a function of time (blue).

III. RESULTS AND DISCUSSION

A. Typical experiment

Figure 2 illustrates the results obtained for a typical impact experiment: a) an image sequence; b) the ratio between the total area covered with water drop S and the initial wetted area S_0 as the function of time with references to the images of the key moments (images A to E); and c) a graph of the ratio of the number of droplets over the initial one (red) and the mean droplet radius (blue) as a function of time.

Figure 2(a) image A corresponds to the initial breath figure formed after a certain condensation time, which is characterized by R_m .

Figure 2(a) images B-C have been obtained at the impact moment, when the magnetic ball is still in contact with the solid surface. If the acceleration of the substrate is large enough, contact lines of most of the droplets are unpinned and droplets start to vibrate. Their radius expand and retract as it has been described by Noblin *et al.* [27]. If droplets are close to each other, they can touch and coalesce into finally giving birth to larger droplets. Multiple droplet coalescence can occur at the same time. This process can be observed on the zoomed part between images A and B (Fig. 2). Therefore, during this first oscillation of the drops, a few coalescence events occur which correspond to the first variation of the wetted area (from images A to B until C) and the decrease in the droplet number on graph in Fig. 2(b).

Figure 2(a) images D-E: The new droplets continue to oscillate forced by the substrate free oscillations (when ball has left the surface), involving new coalescence events. It occurs when two droplets coalesce while oscillating. They will be able to touch, on a second time, other drops. If the drop is far from the others, its radius oscillates between a maximum value to a minimum one until the substrate stop to move.

In the end, there are less droplets but those are bigger than the initial ones, and so the final total wetted area is also smaller [Fig. 2(a) image E]. Finally, in a very short characteristic time (around 20 ms), the number of droplets and the wetted area have been drastically reduced and the droplets size increased.

In the most extreme cases when the initial droplets are large or the acceleration is high enough, we can achieve a state where all the droplets are connected, forming a continuous liquid network, as illustrated in Figs. 3(a) or 3(b), $t=2.5$ ms. This is similar to spinodal dewetting [32–34], demixing, or coarsening patterns [35,36].

We can hence observe three different coalescence patterns for the three accelerations presented: Figure 3(a) liquid film with small dry holes as for $t=1.25$ ms where water cover most of the surface. Figure 3(b) liquid network of long filaments as for $t=2.5$ ms. Figure 3(c) localized coalescence event of few droplets as for $t=1.25, 2.5,$ and 4.75 ms. The full high-speed movies (4000 fps) showing these three experiments are available in Supplemental Material [37].

Due to contact angle hysteresis, when the vibrations are stopped soon after a coalescence event, the final shape of droplets is not always circular. This has been shown in particular in Ref. [5]; we observe the same feature here. In our case, the moderate hysteresis leads, even in case of really strong deformation as in Fig. 3, time $t=4,75$ ms, to a state where most droplets are finally ($t=40$ ms) close to being circular, a few being clearly elliptical.

B. Droplet Number Reduction

We have studied the influence of an impact on a breath figure by comparing the droplet number and the initial mean contact radius before and after the impact. We define the droplet number reduction as $\%DNR = 100 * (1 - N_f/N_i)$, where N_i and N_f are respectively the initial and final number of droplets in the field of view. This number gives information on the number of coalescence and represents in a certain way the efficiency of an impact. A high $\%DNR$ value implies that most droplets have been set in motion and many coalescence events happened, making the impact very efficient.

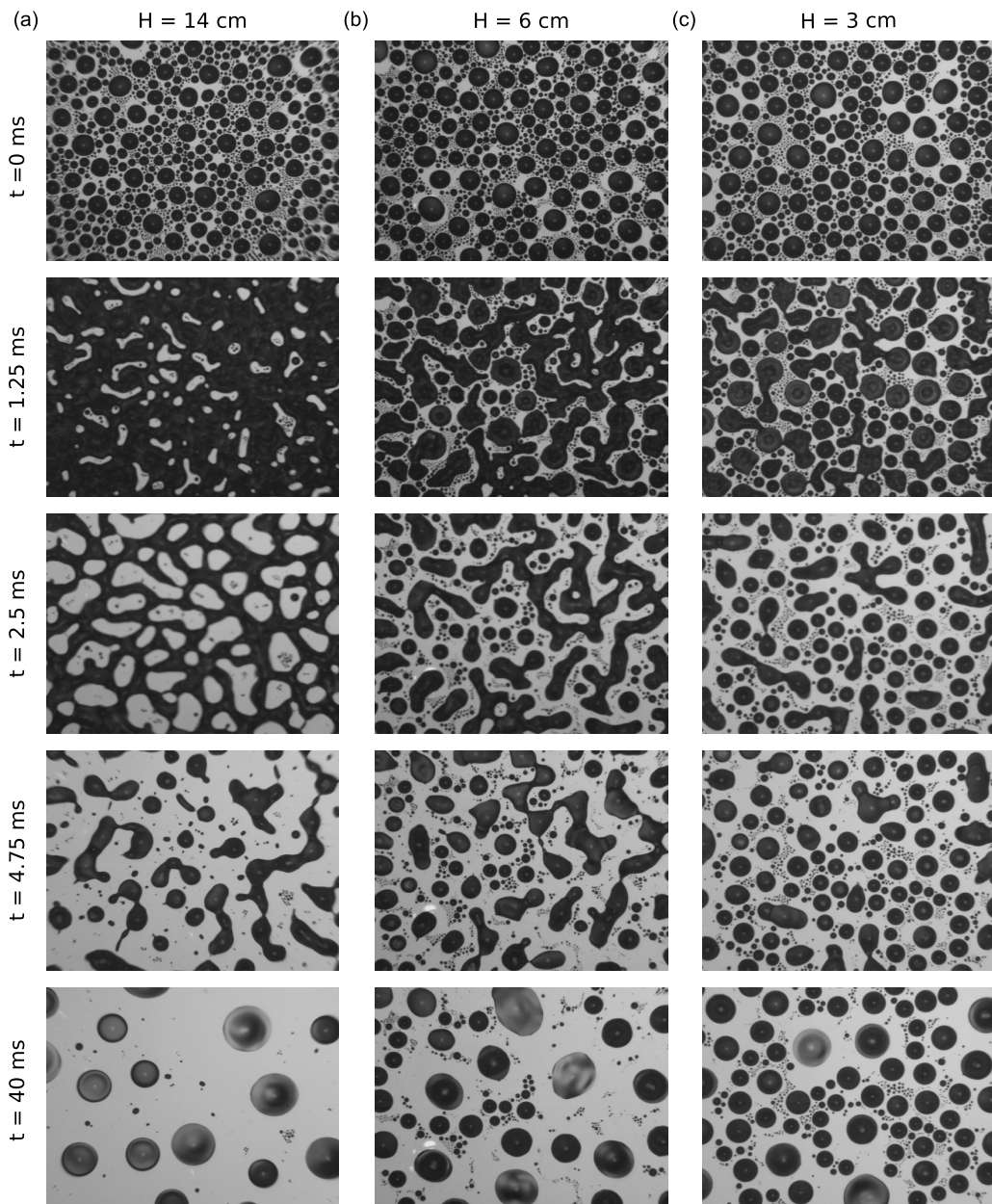


FIG. 3. Breath figure coalescence pattern at various times after impact for three accelerations (varied using height H).

Figure 4 presents the droplet number reduction as a function of their initial mean contact radius R_m , for five different values of substrate acceleration. The acceleration has been varied by two different ways: fixing the dropping height and varying the observation area (full symbols), or by fixing the observation area and varying the dropping height (empty symbols). Each position on the substrate, as explained in the previous section, is characterized by a different acceleration value. The mean contact radius has been varied by changing the condensing time. We can see that for

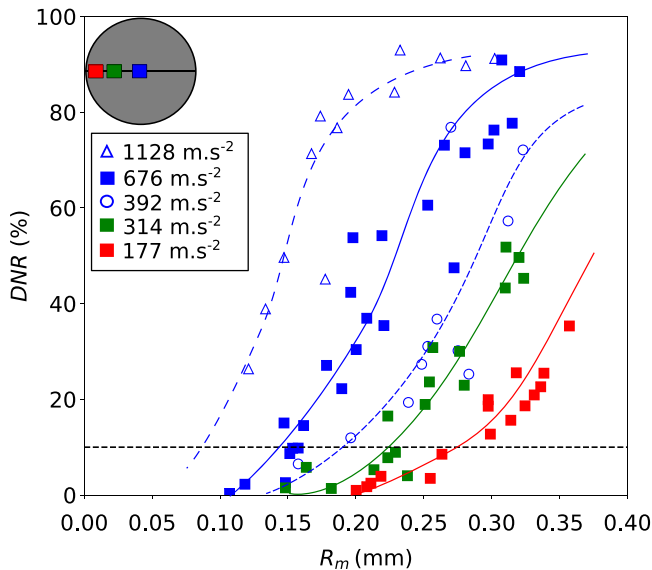


FIG. 4. Droplet number reduction as a function of the initial mean contact radius, under different acceleration. The different curves are tendencies showing the typical variations with threshold and saturation and are only guides for the eye.

each case, the curve follows the same tendency. First, $\%DNR$ is close to zero until the mean contact radius reaches a certain threshold value R_s . Then $\%DNR$ starts to increase linearly until R_m reaches another limit value, when $\%DNR$ is maximal. Furthermore, we can notice that the value of the threshold radius depends on the acceleration. More precisely, the smaller the acceleration is, the larger the drops need to be in order to be able to coalesce with their neighbors. The threshold radius can be explained by the fact that a minimum acceleration is needed in order to unpin contact lines and to involve a sufficient expansion of drop radius to allow coalescence event to occur.

Indeed, Noblin *et al.* [26,27] showed that for a specific frequency there is a threshold acceleration needed to set the contact line into motion. In addition, they show that maximum vibrations of drops are obtained when the excitation frequency is close to the natural frequency of the drop which depends on its size. In our case, there is a wide range of frequencies which allows induction of sufficient movement of drops of different sizes. There are also a few specific frequencies as shown in Fig. 1 which can excite droplets, as long as it is not larger than their natural frequencies. This shows also that we have measured R_s as function of the acceleration by taking the value of R_m from which $\%DNR$ is higher or equal to 10%. This difference in terms of thresholds (that are different and decreasing in terms of R_m for increasing acceleration) could be explained by the acceleration needed to counteract the high surface tension effect acting for these smaller droplet sizes. We propose then to analyze our results in term of an effective Bond number β .

C. Effective Bond number approach

Indeed, β is a dimensionless number measuring the importance of gravity or another external acceleration compared to surface tension force. Hence, one defines an effective Bond number β^* which take the substrate acceleration into account instead of g as :

$$\beta^* = \frac{\Delta\rho a_1 R_m^2}{\gamma}. \quad (1)$$

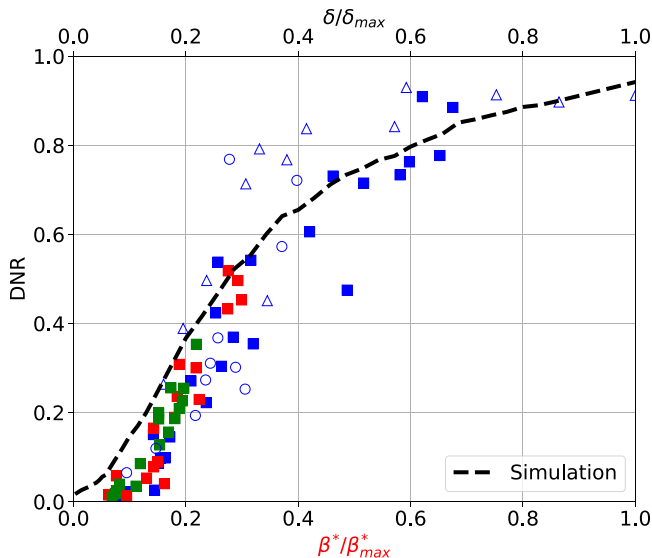


FIG. 5. Symbols: experiments, from the same data set as in Fig. 4, with the same symbol characteristic of the acceleration. The %DNR is plotted as function of the rescaled specific bond number. Dashed line: numerical simulation, the %DNR is plotted as function of the droplet spreading factor δ rescaled with its maximal value (upper horizontal axis showing the same numerical values as for the rescaled Bond Number).

Here $\Delta\rho$ is the difference in density of the two phases (liquid and gas), a_1 is the acceleration of the substrate around the studied area, and R_m is the initial mean contact radius.

Figure 5 presents the %DNR as a function of β^* rescaled by β^*_{max} . It shows that all the curves fall on a single master curve. Interestingly, this representation highlights in a quantitative way the role of droplets radii and substrate acceleration in a simple way through the specific Bond number.

D. Simple Numerical approach

In order to reproduce the experiments presented and especially the curve obtained in Fig. 5, we have performed numerical simulations. The approach is simple and consists of having a finite system made of a few hundreds of droplets, the same as in the experimental window, and describing each droplet i by a circular object [placed at given center of mass (X_i, Y_i) , with radius $r_0(i)$]. These objects correspond at rest to hemispherical droplet of volume $V_i = \frac{2}{3}\pi r_{0,i}^3$. The initial state at $t = 0$ is set from an image of a real breath figure from an experiment. Upon impact at t_{impact} , we assume that the radius r of each droplets is increased by a factor δ varying from 0.1% to 35% of the initial radius $r_i(t_{impact}) = r_{0,i}(1 + \delta)$. This range has been estimated from impact experiments. The coalescence occurs between two drops (i, j) when the condition (of overlapping) $d \leq r_i + r_j$ is verified with d_{ij} the distance between the two droplets, giving birth to a unique droplet : $V_k = V_i + V_j = \frac{2}{3}\pi r_{0,k}^3$, $X = \frac{X_i\rho V_i + X_j\rho V_j}{V_i + V_j}$, and $Y = \frac{Y_i\rho V_i + Y_j\rho V_j}{V_i + V_j}$. If the condition is not met, each corresponding droplet l remains with the radius at $t = t_{impact}$ equal to $r = r_0 + \delta$. After this first iteration, the system keeps on evolving since for $t > t_{impact}$ the new droplets oscillate as $r_k(t) = r_{0,k} + \delta r_{0,k} \cos(\omega(t - t_{impact})) \exp(-(t - t_{impact})/\tau)$. At each following iteration of the simulation, for each droplet, the condition is checked if it were overlapping with another neighboring droplet during the damped oscillations process that last a few periods. These simulations have been realized several times for each value of the radius expansion factor at impact δ . It allows us to explore and multiply the amount of data. We have calculated at the last steps of the simulation (when no more droplets oscillate and eventually coalesce) the number of droplets and measure for

each simulation the $\%DNR$. If we assume that the droplets oscillation amplitude were proportional to the acceleration, then a direct link should exist between δ and β^* . To compare the $\%DNR$ in the experiments and in the simulation, we have plotted in Fig. 5 the curves as a function of the normalized values (β^*/β_{\max}^* and δ/δ_{\max}). This upper and lower axis vary both from 0 to 1. We find again a good agreement between simulation and experiments, obtaining a simulated master curve (dash line) as shown in Fig. 5. We note that there is a deviation at low values, close to the threshold. In the simulation, the approach does not consider contact angle hysteresis effects: i) As soon as two droplets coalesce, they form a new, perfectly circular droplet which would not be the case with hysteresis. ii) The direct correspondence between δ/δ_{\max} and β^*/β_{\max}^* means that even with a tiny value of δ , there will be in the simulation a reduction of the droplet number, but in the experiments with hysteresis, for low value of β , due to the threshold linked to contact angle hysteresis, there is no radius oscillations so strictly no reduction in the droplet number. This explains why for β^*/β_{\max}^* below 0.15 there is a discrepancy with the simulated curve that does not present any threshold and goes to 0 for a null value of δ/δ_{\max} .

IV. CONCLUSION

In conclusion, we have shown that when a plate supporting a breath figure is vibrated through an impact, it may lead to a fast evolution of the droplets pattern. The main parameters explored are the initial mean radius R_m of the large droplets and the substrate's acceleration (a_1). The larger both parameters are, the higher the reduction in droplet number is (and consequently the higher their mean final radius is). The physical explanation for this phenomenon is the radius oscillation of the droplets that can touch their neighbors and coalesce. Each time such an event happens, the number of droplets decreases and the mean radius increases. For sufficiently high accelerations or mean radius, the droplet number can be reduced up to 95%. This is coherent with the fact that there is a threshold acceleration needed to unpin the contact line.

We introduced a specific Bond number β^* built with R_m and a_1 . This allows us to obtain a master curve for the $\%DNR$ that quantitatively gathers all the data and enables predictions.

We compared our experimental results with a numerical approach showing a very good agreement, except at values close to the threshold acceleration since the numerical method does not consider hysteresis effects, consequently not showing thresholds effects, but having the exact same behavior for large amplitude of vibrations.

This method can be very useful for dew recovery systems, improving the efficiency by accelerating the droplets growth from the coalescence of many droplets, in a very short time compared to the natural growth.

This can be interesting to help removing droplets from a substrate, but also as a new fundamental system of interest since it gives another way to induce the droplet growth and to understand the link between hysteresis, droplets coalescence on a multi droplets systems. In such systems, new behaviors can emerge and should be new topics to explore. In particular, to make links with spinodal decomposition and also for more many-droplets interactions (not only 2-body system). The dynamics of large filaments of liquids as a function of wetting characteristics of the surface is also an interesting perspective.

ACKNOWLEDGMENTS

We would like to thank Julien Sylvestre for his help and The Centre National de la Recherche Scientifique (CNRS) and Université Côte d'Azur (UCA) for funding.

[1] D. Beysens, A. Steyer, P. Guenoun, D. Fritter, and C. M. Knobler, How does dew form?, *Phase Transitions* **31**, 219 (1991).

- [2] F. Family and P. Meakin, Kinetics of droplet growth processes: Simulations, theory, and experiments, *Phys. Rev. A* **40**, 3836 (1989).
- [3] B. Briscoe and K. Galvin, An experimental study of the growth of breath figures, *Colloids Surf.* **56**, 263 (1991).
- [4] D. Fritter, C. M. Knobler, D. Roux, and D. Beysens, Computer simulations of the growth of Breath figures, *J. Stat. Phys.* **52**, 1447 (1988).
- [5] H. Zhao and D. Beysens, From droplet growth to film growth on a heterogeneous surface: Condensation associated with a wettability gradient, *Langmuir* **11**, 627 (1995).
- [6] G. Widawski, M. Rawiso, and B. François, Self-organized honeycomb morphology of starpolymer polystyrene films, *Nature (London)* **369**, 387 (1994).
- [7] A. Böker, Y. Lin, K. Chiapperini, R. Horowitz, M. Thompson, V. Carreon, T. Xu, C. Abetz, H. Skaff, A. D. Dinsmore, T. Emrick, and T. P. Russell, Hierarchical nanoparticle assemblies formed by decorating breath figures, *Nat. Mater.* **3**, 302 (2004).
- [8] M. Muselli, D. Beysens, J. Marcillat, I. Milimouk, T. Nilsson, and A. Louche, Dew water collector for potable water in Ajaccio (Corsica Island, France), *Atmos. Res.* **64**, 297 (2002).
- [9] D. Beysens, *Dew Water*, (River Publishers, Gistrup, 2018)
- [10] D. Beysens, *The Physics of Dew, Breath Figures and Dropwise Condensation*, 1st ed., Lecture Notes in Physics No. Vol 994 (Springer Verlag, Berlin, 2022).
- [11] J. E. Castillo, J. A. Weibel, and S. V. Garimella, The effect of relative humidity on dropwise condensation dynamics, *Int. J. Heat Mass Transf.* **80**, 759 (2015).
- [12] K. K. Varanasi, M. Hsu, N. Bhate, W. Yang, and T. Deng, Spatial control in the heterogeneous nucleation of water, *Appl. Phys. Lett.* **95**, 094101 (2009).
- [13] A. Lee, M.-W. Moon, H. Lim, W.-D. Kim, and H.-Y. Kim, Water harvest via dewing, *Langmuir* **28**, 10183 (2012).
- [14] D. Nioras, K. Ellinas, V. Constantoudis, and E. Gogolides, How different are fog collection and dew water harvesting on surfaces with different wetting behaviors?, *ACS Appl. Mater. Interfaces* **13**, 48322 (2021).
- [15] T. Mouterde, G. Lehoucq, S. Xavier, A. Checco, C. T. Black, A. Rahman, T. Midavaine, C. Clanet, and D. Quéré, Antifogging abilities of model nanotextures, *Nat. Mater.* **16**, 658 (2017).
- [16] T. Mouterde, T.-V. Nguyen, H. Takahashi, C. Clanet, I. Shimoyama, and D. Quéré, How merging droplets jump on a superhydrophobic surface: Measurements and model, *Phys. Rev. Fluids* **2**, 112001(R) (2017).
- [17] I. O. Ucar and H. Y. Erbil, Dropwise condensation rate of water breath figures on polymer surfaces having similar surface free energies, *Appl. Surf. Sci.* **259**, 515 (2012).
- [18] M. M. Garimella, S. Koppu, S. S. Kadlaskar, V. Pillutla, Abhijeet, and W. Choi, Difference in growth and coalescing patterns of droplets on bi-philic surfaces with varying spatial distribution, *J. Colloid Interface Sci.* **505**, 1065 (2017).
- [19] N. Pionnier, J. Vera, E. Contraires, S. Benayoun, R. Berger, and S. Valette, The effect of the orientation and the height of periodic sub-micrometric texturing on dropwise condensation, *J. Colloid Interface Sci.* **526**, 184 (2018).
- [20] M.-G. Medici, A. Mongruel, L. Royon, and D. Beysens, Edge effects on water droplet condensation, *Phys. Rev. E* **90**, 062403 (2014).
- [21] C. Furmidge, Studies at phase interfaces. I. sliding of liquid drops on solid surfaces and a theory for spray retention, *J. Colloid Sci.* **17**, 309 (1962).
- [22] E. Pierce, F. J. Carmona, and A. Amirfazli, Understanding of sliding and contact angle results in tilted plate experiments, *Colloids and Surfaces A-Physicochemical and Engineering aspects* **323**, 73 (2008).
- [23] N. Kapur and P. H. Gaskell, Morphology and dynamics of droplet coalescence on a surface, *Phys. Rev. E* **75**, 056315 (2007).
- [24] A. Lai, N. Bremond, and H. A. Stone, Separation-driven coalescence of droplets: an analytical criterion for the approach to contact, *J. Fluid Mech.* **632**, 97 (2009).
- [25] X. Niu, S. Gulati, J. B. Edel, and A. J. deMello, Pillar-induced droplet merging in microfluidic circuits, *Lab Chip* **8**, 1837 (2008).
- [26] X. Noblin, A. Buguin, and F. Brochard-Wyart, Vibrated sessile drops: Transition between pinned and mobile contact line oscillations, *The European Physical Journal E* **14**, 395 (2004).

- [27] X. Noblin, A. Buguin, and F. Brochard-Wyart, Vibrations of sessile drops, *Eur. Phys. J.: Spec. Top.* **166**, 7 (2009).
- [28] S. Daniel, M. K. Chaudhury, and P.-G. de Gennes, Vibration-actuated drop motion on surfaces for batch microfluidic processes, *Langmuir* **21**, 4240 (2005).
- [29] X. Noblin, R. Kofman, and F. Celestini, Ratchetlike motion of a shaken drop, *Phys. Rev. Lett.* **102**, 194504 (2009).
- [30] Y. Lu, A. Sur, C. Pascente, S. Ravi Annapragada, P. Ruchhoeft, and D. Liu, Dynamics of droplet motion induced by electrowetting, *Int. J. Heat Mass Transf.* **106**, 920 (2017).
- [31] W. Soedel, *Vibrations of Shells and Plates*, Third Edition (Marcel Dekker inc., New York, 2004).
- [32] F. Vandenbrouck, M. P. Valignat, and A. M. Cazabat, Thin Nematic Films: Metastability and Spinodal Dewetting, *Phys. Rev. Lett.* **82**, 2693 (1999).
- [33] R. Seemann, S. Herminghaus, and K. Jacobs, Gaining control of pattern formation of dewetting liquid films, *J. Phys.: Condens. Matter* **13**, 4925 (2001).
- [34] J. Becker, G. Grün, R. Seemann, H. Mantz, K. Jacobs, K. R. Mecke, and R. Blossey, Complex dewetting scenarios captured by thin-film models, *Nat. Mater.* **2**, 59 (2003).
- [35] A. J. Bray, Theory of phase-ordering kinetics, *Adv. Phys.* **43**, 357 (1994).
- [36] R. Mukherjee and A. Sharma, Instability, self-organization and pattern formation in thin soft films, *Soft Matter* **11**, 8717 (2015).
- [37] See Supplemental Material at <http://link.aps.org/supplemental/10.1103/PhysRevFluids.8.013601> for 3 high speed movies (4000 fps) of a breath figure submitted to vibrations of its support due to an impacting bead. the movies correspond to figure 3. the falling heights are here 3, 6 and 14 cm, respectively for the files pc-3cm.mp4, pc-6cm.mp4 and pc-14cm.mp4.

Correction: The author names were not presented as intended and have been expanded to include full first names. The name of the institution in the affiliation was presented incorrectly and has been fixed.